Enhanced local magnetization by interface engineering in perovskite-type correlated oxide heterostructures

Enhanced local magnetization by interface engineering in perovskite-type correlated oxide heterostructures

Mark Huijben, Yaohua Liu, Hans Boschker, Valeria Lauter, Ricardo Egoavil, Jo Verbeeck, Suzanne G.E. te Velthuis, Guus Rijnders, and Gertjan Koster*

Dr. Mark Huijben, Dr. Hans Boschker, Prof. dr. Guus Rijnders, and Dr. Gertjan Koster
Faculty of Science and Technology and MESA+ Institute for Nanotechnology, University of Twente, 7500 AE, Enschede, The Netherlands
Email: m.huijben@utwente.nl
Dr. Yaohua Liu, Dr. Suzanne G.E. te Velthuis
Materials Science Division, Argonne National Laboratory, Argonne IL, USA
Dr. Hans Boschker
Max Planck Institute for Solid State Research, 70569 Stuttgart, Germany
Dr. Valeria Lauter
Neutron Sciences Directorate, Oak Ridge National Laboratory, Oak Ridge TN, USA
Ricardo Egoavil, Prof. dr. Jo Verbeeck
Electron Microscopy for Materials Science (EMAT), University of Antwerp, 2020 Antwerp, Belgium

Keywords: interface engineering, oxide heterostructures, magnetism, epitaxy, perovskite

Correlated oxide materials attract significant attention as the interplay between their charge, spin, orbital and lattice degrees of freedom gives rise to a wide variety of functional properties. This research field is even further enriched by the controlled formation of highly ordered oxide heterostructures in which new functionalities emerge at the interfaces.[1,2] Usually reduced physical properties in ultrathin correlated oxide films are macroscopically measured and attributed to the interfaces, which is referred to as 'dead-layers'. These have been observed in perovskite-type transition-metal oxide heterostructures, such as reduced dielectric ($SrTiO_3$),[3] ferroelectric ($BaTiO_3$ and $PbTiO_3$)[4] and ferromagnetic ($SrRuO_3$ and $La_{0.67}Sr_{0.33}MnO_3$)[5,6] properties. The presence of these dead-layers results in reduced performance of devices due to the local changes in material properties at the interfaces. In perovskite-type transition-metal oxides the interfacial properties depend strongly on the precise atomic stacking sequence at the interface, e.g. the termination dependent conducting or insulating behavior of the $LaAlO_3/SrTiO_3$ and $LaVO_3/SrTiO_3$ interfaces[7–9] and the

termination dependent exchange bias in $La_{0.67}Sr_{0.33}MnO_3/BiFeO_3$ heterostructures.[10] These interfaces are created by the stacking of two different correlated oxide materials and the obtained interfacial properties are serendipitous. To fully exploit interfacial phenomena, the capability of controlled growth of interfacial atomic stacking has to be combined with local probing of the interfacial properties to enable true interface engineering.

The interface between the ferromagnetic metallic $La_{0.67}Sr_{0.33}MnO_3$ (LSMO) and the insulating $SrTiO_3$ (STO) has been well studied, because of the relevance in various devices, such as diodes,[11,12] transistors[13] and magnetic tunnel junctions.[14] Although working devices have been reported, it is well known that the electrical conductivity and magnetization of the LSMO layer can be strongly reduced at the interface to STO.[6] Although the precise origin of the dead-layer is still a topic of discussion,[15–18] recent progress has been made in the realization of the importance of the microstructure,[19] the beneficial effect of contact to metallic reservoirs at the interface[20] and the identification of competing misfit relaxation mechanisms.[21] A variety of experiments and theoretical models point towards the importance of the structural coupling of the oxygen octahedral rotations that governs the local crystal structure of the LSMO at the interface.[22–27] Various studies have used interface engineering to improve the devices, for example by inserting either a 2 unit cell $LaMnO_3$ layer to compensate for an observed valence change[28,29] or a single SrO layer to modify the Schottky barrier height of the devices.[12,13] However, only recently it has been shown that the fundamental symmetry change of the polarization at the interface, i.e. the polar discontinuity, can be prevented by inserting a single $La_{0.33}Sr_{0.67}O$ layer, which eliminates the local atomic reconstruction and results in improved interface magnetization and electrical conductivity.[25]

Macroscopic characterization of the magnetic and electrical properties of single LSMO/STO bilayer systems have clearly demonstrated the enhancement in magnetization and electrical conductivity when a single $La_{0.33}Sr_{0.67}O$ layer is inserted at the interface.[25] Furthermore, scanning transmission electron microscopy combined with electron energy loss

spectroscopy (STEM-EELS) was used to study the local structural changes at the interfaces. However, the dependence of the local magnetization on the interface engineering remained unknown. Here, we have used a combination of polarized neutron reflectometry (PNR)[30,31] and scanning transmission electron microscopy to study the local interface magnetization in LSMO/STO multilayer systems without and with interface engineering by insertion of $La_{0.33}Sr_{0.67}O$ layers in the latter case. We demonstrate true interface engineering with the successful combination of controlled growth of interfacial atomic stacking and local magnetic probing, resulting in equal LSMO magnetic and chemical layer thicknesses, thus optimal interfacial magnetization for device applications.[11–14]

To increase the signal at high momentum transfer Q_z and the sensitivity to the interfaces for PNR, the high quality LSMO/STO bilayer was repeated 5 times in a heterostructure system (see **Figure 1**). Heterostructures with and without interface engineering were grown by pulsed laser deposition (PLD) at 800 ^{o}C in an oxygen environment of 0.27 mbar, as described previously.[25,32] Reflective high-energy electron diffraction (RHEED) during growth indicated layer-by-layer growth mode for the complete heterostructures. The non-interface engineered (non-IE) heterostructure consisted of a TiO_2-terminated STO substrate on which a LSMO layer with a thickness of 8 unit cells (31.0 Å) was deposited, followed by a STO layer with a thickness of 5 unit cells (19.5 Å), see Figure 1a. In order to realize the interface-engineered (IE) heterostructure, first a single unit cell layer of $La_{0.33}Sr_{0.67}MnO_3$ is grown on the substrate, followed by the growth of 7 unit cell layers of LSMO, then a single $La_{0.33}Sr_{0.67}TiO_3$ layer and finally 4 unit cell layers of STO, see Figure 1b. The IE heterostructure then has an atomic stacking sequence at all interfaces of SrO-TiO_2-$La_{0.33}Sr_{0.67}O$-MnO_2-$La_{0.67}Sr_{0.33}O$, where the polar discontinuity is absent and no driving force for reconstruction exists. This deposition sequence results in heterostructures in which each bilayer contains 8 layers of Mn ions, which can therefore be compared to the 8 unit cell layer LSMO/STO structure without the interface engineering. The deposited structure is confirmed

by scanning transmission electron microscopy (STEM) performed on the Qu-Ant-Em instrument at the University of Antwerp. The instrument consists of a double corrected FEI Titan G3 electron microscope operating at 120 kV for high angle annular dark field (HAADF) imaging, while the electron energy loss spectroscopy (EELS) measurements were performed at 300 kV. High angle annular dark field STEM images are presented in Figure 1 and agree well with the nominal growth sequence. Quantitative elemental profiles for La and Mn are determined by EELS of the atomic columns within the first LSMO layer on the STO substrate for both types of heterostructures, as shown in **Figure 2**. These normalized core-loss signals for La $M_{4,5}$ (red) and Mn $L_{2,3}$ (black) edges are in good agreement with the ideal model for the atomic layering sequence in both heterostructures as can be seen in the corresponding top schematic representations. Precise quantification of the stoichiometry and chemical volumes of the layers from this data is hindered by channeling effects caused by the zone axis conditions required for atomic resolution mapping. We therefore will need to obtain this information from an extra free parameter in fitting the PNR data as will be discussed further on. The deposition of a single $La_{0.33}Sr_{0.67}TiO_3$ layer on top of the LSMO layer will lead to a second interface with half the amount of La atoms as compared to a standard LSMO layer. This will lead to symmetric interfaces, as can be seen in Figure 2, in which a $La_{0.33}Sr_{0.67}O$ atomic layer forms the interface with the subsequent TiO_2 atomic layer. These IE heterostructures show a more gradual La transition at the interface, as measured by STEM-EELS, in comparison to non-IE heterostructures. These observations agree very well with the intended designs in sample stacking sequence as can be seen in the schematic representations in Figure 2. This interface engineering in IE heterostructures influences the local magnetization as the final MnO_2 atomic layer on top of each LSMO layer is now embedded in between two (La,Sr)O layers, in contrast to non-IE heterostructures, see Figure 2.

The polarized neutron reflectivity (PNR) measurements were performed on the Magnetism Reflectometer (BL-4A) of the Spallation Neutron Source at Oak Ridge National

Laboratory.[33] Both types of heterostructures were measured at a temperature of 120 K after field cooling in 1 T. This temperature was chosen to maximize the magnetic moment, while staying above the structural transition of the $SrTiO_3$ substrate[34,35] that tends to roughen the surface by formation of grains with a surface that tilts out of the plane[36]. Furthermore, the chosen measurement temperature of 120 K is far below the Curie temperatures of 290 K and 270 K for superlattices with and without interface engineering, respectively. An in-plane magnetic field of 1 T was applied to saturate all magnetization parallel to the applied field, thereby eliminating contributions to spin-flip scattering. By polarizing the incident neutron beam, the two scattered neutron states (R^+ for spin up and R^- for spin down) were measured as a function of momentum transfer Q_z. The instrument had a neutron wavelength band ranging from 0.18 - 0.45 nm and the time-of-flight method was used to discriminate the neutron wavelengths (λ) as they reach the detector. In order to cover the desired Q_z range, data was collected at different incident angles (θ). The obtained PNR data are shown in **Figure 3** along with X-ray reflectivity data, collected using a Cu-Kα source at room temperature at Argonne National Laboratory.

The neutron and X-ray reflectivity data have been fitted to a model of the depth profile of the scattering length densities (SLD) to determine the local structural and magnetic properties within the LSMO/STO heterostructures. For X-ray reflectivity this scattering length density is proportional to the element specific scattering factors f' and f''. For neutron reflectivity there are two contributions: a nuclear one that like the X-ray SLD depends on the chemical atomic structure with a predominant coherent scattering length b for each element[37,38] in the material, and a magnetic one that is directly proportional to the magnetic induction B and hence the magnetization M. The values of the X-ray and nuclear SLDs can be calculated using known tabulated values of the f', f'', and b for each element and then taking composition and density (i.e. unit cell volume) into account. Each layer in the system and the substrate are described in

the model by the chemical (i.e. structural) parameters: real part of X-ray electron density (f'), imaginary part of X-ray electron density (f"), real part of the neutron nuclear SLD, chemical thickness t_n, chemical roughness σ_n and magnetic parameters: neutron magnetic SLD, magnetic thickness t_m, magnetic roughness σ_m. The neutron absorption cross-section for the materials in these heterostructures is negligible.[39,40] While in typical SLD modeling one value per layer is used for the thickness and roughness (chemical=magnetic), here a distinction is made between the chemical (i.e. nuclear) thickness and roughness and the magnetic values as for the interface-engineered heterostructure it is expected that the scattering length density of the added $La_{0.33}Sr_{0.67}O$ interfacial monolayer is indistinguishable from the rest of the LSMO layer, but the corresponding magnetic properties are different. The modeling is limited by the use of Gaussian profiles instead of experimentally measured chemical profiles by EELS. Analysis of the fits will provide reliable information on the width of the chemical and magnetic profiles, the relative shift of one with respect to the other, and the absolute heights of the chemical and magnetic profiles in the different layers.

For these experiments, the combined fitting of the X-ray and neutron reflectivity data is important because, due to the relatively small difference in the neutron nuclear SLDs of STO and LSMO, the features of the PNR data are dominated by the variations in the magnetic SLD. In particular the shape and height of the superlattice Bragg peaks around Q_z = 0.12 - 0.13 $Å^{-1}$ are sensitive to the interfacial magnetic variations. The fit to the X-ray reflectivity data predominately determined the structural information. The neutron and X-ray reflectivity data were fit simultaneously, using the same chemical thicknesses and roughnesses, to limit the number of fitting parameters. The real part of X-ray SLD and real part of neutron nuclear SLD were also linked together by a fixed ratio, motivated by the assumption that any variation of these values is the result of a change in unit cell volume (or density), which would impact both parameters equally. The combined fitting results of the neutron and X-ray reflectivity data are shown in Figure 3 in which a good agreement can be observed for the

optimized model with the PNR measurements as well as with the X-ray reflectivity measurements.

The details of the optimized models for the non-interface-engineered heterostructure (**Figures 4a, 4c and 4e**) and the interface-engineered heterostructure (Figures 4b, 4d and 4f) are shown for the structural as well as the magnetic information. In these figures the dashed lines represent the SLD profiles as the solid lines but without taking the roughness into account (a so-called box model) and thereby they more clearly visualize the boundaries of each layer. These profiles show that the topmost STO and LSMO layers exhibited different structural properties, most likely due to relaxation at the surface. However, all other four buried LSMO/STO bilayers showed to be structurally equal as demonstrated by showing the first (L1) and fourth (L4) LSMO layer in respectively Figures 4c/4e and 4d/4f. The chemical thicknesses of both heterostructures are in good agreement with the EELS analysis in Figure 2. The transition of the chemical profiles at the interfaces in the IE heterostructure are wider than that in the non-IE heterostructure, consistent with the intended more gradual La distribution in the design of the IE heterostructure. The magnetic roughnesses, in contrast, are similar in both heterostructures.

Most importantly, for the non-interface-engineered (non-IE) heterostructure a clear 5.5 Å ±1.0 Å difference between the magnetic and chemical thickness of the LSMO layer was observed (Figures 4c and 4e). The optimal model indicates that only the top part of each LSMO layer was strongly magnetically reduced. We have considered several alternative models. In the first one, the magnetic thickness is constrained to be equal to the chemical thickness, and varying only the other magnetic parameters resulted in an increase of the error χ^2 of the neutron data fit by 36 %. Applying the same constraint, but allowing magnetic and structural parameters to vary, increased the error χ^2 of the fits of the neutron data and X-ray data by 14 % and 19 %, respectively. More importantly, both cases significantly overestimate the average magnetization of the sample by 15 % as obtained by vibrating sample

magnetometry (VSM) measurement. In the second model, we put the magnetically dead layer completely at the bottom interface, which increases the error χ^2 of both the neutron and x-ray data by 36 % and overestimates the average saturation magnetization by 10 %. Therefore, these two models can be definitively excluded. Finally, a model was fitted assuming equally sized dead layers at the top and bottom of each LSMO layer. Variation of the magnetic and structural parameters resulted in a slight improvement of 4 % in the error χ^2 of the neutron data and an increase of 11 % in the error χ^2 of the X-ray data. The model also yields a total 5 Å magnetically dead region (2.5 Å each at top and bottom interfaces), similar to the optimal model. At the same time, the average magnetization agrees with the optimal model as well. Therefore, the difference between the last model (equal magnetically dead interfaces) and the optimal model (larger magnetically dead layer at the top interface) is less significant, and the practical resolution of our PNR experiment limits us to resolve it, unless we have complementary information from other techniques. This is in good agreement with previous observation that La surplus at the interface does not deteriorate the magnetism.[6] On the other hand, at the top interface, a reduction of the magnetization is found in a layer where Mn exists, therefore a true magnetic dead-layer LSMO only resides at the top interface. Overall, in the non-interface engineered heterostructure, the magnetic thickness is ~ 5 Å less than the chemical thickness, and there is at least a magnetically reduced region at the top, and possibly at the bottom, the combination of which is 5.5 Å ± 1.0 Å thick.

In contrast, the interface-engineered (IE) heterostructure demonstrated an equal magnetic and chemical thickness of the LSMO layer (Figures 4d and 4f). The integrated magnetization at 120 K over the 8 unit cells LSMO layer, extracted from the PNR data, is ~3.3 μB/Mn for the heterostructure with interface engineering, while a heterostructure without interface engineering exhibited a magnetization of only ~2.8 μB/Mn. The absolute magnetization values extracted from PNR are confirmed by VSM measurements and the observed

magnetization enhancement of 18 % is in very good agreement with the previously observed increase in magnetization of a single LSMO/STO bilayer when interface engineering was applied.[25]

In conclusion, we have investigated the origin of the enhanced magnetization in interface engineered LSMO/STO heterostructures by using polarized neutron reflectometry for probing the local profile of magnetization. From fitting of the neutron and X-ray reflectivity data to a model of the depth profile of the scattering length densities, we determined the local variations in structural and magnetic properties within the LSMO/STO heterostructures. These results provide strong evidence of the elimination of a magnetic dead-layer at the LSMO/STO interface when applying interface engineering by incorporating of a single $La_{0.33}Sr_{0.67}O$ layer, which leads to embedding of the interfacial MnO_2 atomic layer in between two (La,Sr)O layers. Furthermore, both the interface asymmetry of the magnetically reduced layer in the non-IE heterostructure and the absence of the dead-layer in the IE heterostructure confirm the reconstructions induced by the polar discontinuity at the interface as the origin of the former magnetic dead-layer at LSMO/STO interfaces. The capability of controlled growth of interfacial atomic stacking in combination with local probing of the interfacial properties enables true interface engineering, leading towards improved device applications of correlated oxide heterostructures.

Acknowledgements
This work is supported by the Dutch Science Foundation (NWO) and the Dutch Nanotechnology programme NanoNed. Work at Argonne National Laboratory was supported by the U.S. Department of Energy, Office of Science, Basic Energy Sciences, Materials Sciences and Engineering Division. Part of the research conducted at ORNL's Spallation Neutron Source was sponsored by the Scientific User Facilities Division, Office of Basic Energy Sciences, US Department of Energy. H.B. gratefully acknowledges discussions with E. Benckiser. The Qu-Ant-EM microscope was partly funded by the Hercules fund from the Flemish Government. The electron microscopy part of the work was supported by funding from the European Research Council under the 7th Framework Program (FP7), ERC grant Na¸ 246791 - COUNTATOMS and ERC Starting Grant 278510 VORTEX. Funding from the European Union Council under the 7th Framework Program (FP7) grant nr NMP3-LA-2010-246102 IFOX and the contract for an Integrated Infrastructure Initiative. Reference No.

312483-ESTEEM2 is also acknowledged. The Fund for Scientific Research Flanders is acknowledged for FWO project G.0044.13N.

Received: ((will be filled in by the editorial staff))
Revised: ((will be filled in by the editorial staff))
Published online: ((will be filled in by the editorial staff))

References

[1] P. Zubko, S. Gariglio, M. Gabay, P. Ghosez, J.-M. Triscone, *Annual Review of Condensed Matter Physics*, **2011**, *2*, 141–165.

[2] H.Y. Hwang, Y. Iwasa, M. Kawasaki, B. Keimer, N. Nagaosa, Y. Tokura, *Nature Mater.* **2012**, *11*, 103–113.

[3] M. Stengel, N.A. Spaldin, *Nature* **2006**, *443*, 679–682.

[4] M. Stengel, D. Vanderbilt, N.A. Spaldin, *Nature Mater.* **2009**, *8*, 392–397.

[5] G. Koster, L. Klein, W. Siemons, G. Rijnders, J.S. Dodge, C.B. Eom, D.H.A. Blank, M.R. Beasley, *Rev. Mod. Phys.* **2012**, *84*, 253.

[6] J.J. Kavich, M.P. Warusawithana, J.W. Freeland, P. Ryan, X. Zhai, R.H. Kodama, J.N. Eckstein, *Phys. Rev. B* **2007**, *76*, 014410.

[7] A. Ohtomo, H.Y. Hwang, *Nature* **2004**, *427*, 423–426.

[8] M. Huijben, A. Brinkman, G. Koster, G. Rijnders, H. Hilgenkamp, D.H.A. Blank, *Adv. Mater.* **2009**, *21*, 1665–1677.

[9] Y. Hotta, T. Susaki, H.Y. Hwang, *Phys. Rev. Lett.* **2007**, *99*, 236805.

[10] P. Yu, W. Luo, D. Yi, J.X. Zhang, M.D. Rossell, C.-H. Yang, L. You, G. Singh-Bhalla, S.Y. Yang, Q. He, Q.M. Ramasse, R. Erni, L.W. Martin, Y.H. Chu, S.T. Pantelides, S.J. Pennycook, R. Ramesh, *Proc. Nat. Acad. Sci. USA* **2012**, *109*, 9710–9715.

[11] F.M. Postma, R. Ramaneti, T. Banerjee, H. Gokcan, E. Haq, D.H.A. Blank, R. Jansen, J.C. Lodder, *J. Appl. Phys.* **2004**, *95*, 7324–7326.

[12] Y. Hikita, M. Nishikawa, T. Yajima, H.Y. Hwang, *Phys. Rev. B* **2009**, *79*, 073101.

[13] T. Yajima, Y. Hikita, H.Y. Hwang, *Nature Mater.* **2011**, *10*, 198–201.

[14] J.Z. Sun, D.W. Abraham, R.A. Rao, C.B. Eom, *Appl. Phys. Lett.* **1999,** *74*, 3017–3019.

[15] H. Kumigashira, A. Chikamatsu, R. Hashimoto, M. Oshima, T. Ohnishi, M. Lippmaa, H. Wadati, A. Fujimori, K. Ono, M. Kawasaki, H. Koinuma, *Appl. Phys. Lett.* **2006**, *88*, 192504.

[16] A. Tebano, C. Aruta, S. Sanna, P.G. Medaglia, G. Balestrino, A.A. Sidorenko, R. De Renzi, G. Ghiringhelli, L. Braicovich, V. Bisogni, N.B. Brookes, *Phys. Rev. Lett.* **2008**, *100*, 137401.

[17] R. Herger, P.R. Willmott, C.M. Schlepuetz, M. Bjoerck, S.A. Pauli, D. Martoccia, B.D. Patterson, D. Kumah, R. Clarke, Y. Yacoby, M. Doebeli, *Phys. Rev. B* **2008**, *77*, 085401.

[18] M. Huijben, L.W. Martin, Y.H. Chu, M.B. Holcomb, P. Yu, G. Rijnders, D.H.A. Blank, R. Ramesh, *Phys. Rev. B* **2008**, *78*, 094413.

[19] L. Fitting Kourkoutis, J.H. Song, H.Y. Hwang, D.A. Muller, *Proc. Nat. Acad. Sci. USA* **2010**, *107*, 11682–11685.

[20] M. Ziese, F. Bern, E. Pippel, D. Hesse, I. Vrejoiu, *Nano Lett.* **2012**, *12*, 4276–4281.

[21] F. Sandiumenge, J. Santiso, L. Balcells, Z. Konstantinovic, J. Roqueta, A. Pomar, J. Pedro Espinos, B. Martinez, *Phys. Rev. Lett.* **2013**, *110*, 107206.

[22] J.M. Pruneda, V. Ferrari, R. Rurali, P.B. Littlewood, N.A. Spaldin, E. Artacho, *Phys. Rev. Lett.* **2007**, *99*, 226101.

[23] J. He, A. Borisevich, S.V. Kalinin, S.J. Pennycook, S.T. Pantelides, *Phys. Rev. Lett.* **2010**, *105*, 227203.

[24] A.X. Gray, C. Papp, B. Balke, S.-H. Yang, M. Huijben, E. Rotenberg, A. Bostwick, S. Ueda, Y. Yamashita, K. Kobayashi, E.M. Gullikson, J.B. Kortright, F.M.F. de Groot, G. Rijnders, D. H. A. Blank, R. Ramesh, C. S. Fadley, *Phys. Rev. B* **2010**, *82*, 205116.

[25] H. Boschker, J. Verbeeck, R. Egoavil, S. Bals, G. van Tendeloo, M. Huijben, E.P. Houwman, G. Koster, D.H.A. Blank, G. Rijnders, *Adv. Func. Mater.* **2012**, *22*, 2235–2240.

[26] H. Boschker, J. Kautz, E.P. Houwman, W. Siemons, D.H.A. Blank, M. Huijben, G. Koster, A. Vailionis, G. Rijnders, *Phys. Rev. Lett.* **2012**, *109*, 157207.

[27] A.Y. Petrov, X. Torrelles, A. Verna, H. Xu, A. Cossaro, M. Pedio, J. Garcia-Barriocanal, G.R. Castro, B.A. Davidson, *Adv. Mater.* **2013**, *25*, 4043–8.

[28] H. Yamada, Y. Ogawa, Y. Ishii, H. Sato, M. Kawasaki, H. Akoh, Y. Tokura, *Science* **2004**, *305*, 646–648.

[29] Y. Ishii, H. Yamada, H. Sato, H. Akoh, Y. Ogawa, M. Kawasaki, Y. Tokura, *Appl. Phys. Lett.* **2006**, *89*, 042509.

[30] G.P. Felcher, R.O. Hilleke, R.K. Crawford, J. Haumann, R. Kleb, G. Ostrowski, *Rev. Sci. Instrum.* **1987**, *58*, 609–619.

[31] M.R. Fitzsimmons, C. Majkrzak, *Modern Techniques for Characterizing Magnetic Materials*, (Ed.: Y. Zhu), Springer, New York, **2005**, 107–155.

[32] H. Boschker, M. Huijben, A. Vailionis, J. Verbeeck, S. van Aert, M. Luysberg, S. Bals, G. van Tendeloo, E.P. Houwman, G. Koster, D.H.A. Blank, G. Rijnders, *J. Phys. D Appl. Phys.* **2011**, *44*, 205001.

[33] V. Lauter, H. Ambaye, R. Goyette, W.-T. Hal Lee, A. Parizzi, *Physica B: Cond. Matt.***2009**, *404*, 2543–2546.

[34] G. Shirane, Y. Yamada, *Phys. Rev.* **1969**, *177*, 858.

[35] F.W. Lytle, *J. Appl. Phys.* **1964**, *35*, 2212.

[36] M. Honig, J. A. Sulpizio, J. Drori, A. Joshua, E. Zeldov and S. Ilani, *Nature Mater.* **2013**, 12, 1112-1118.

[37] B.L. Henke, E.M. Gullikson, J.C. Davis, *At. Data Nucl. Data Tables* **1993**, *54*, 181–342.

[38] H. Rauch, W. Waschkowski, *Neutron Data Booklet*, vol. 58 (Eds: A.J. Dianoux, G. Lander), Old City Publishing, Philadelphia, **2003**, Ch. 1.1.

[39] E. Segre, *Experimental Nuclear Physics*, vol. 2, John Wiley & Sons, New York, **1953**.

[40] S.F. Mughabghab, *Atlas of Neutron Resonances, Resonance Parameters and Neutron Cross Sections Z = 1-100*, Elsevier, New York, **2006**.

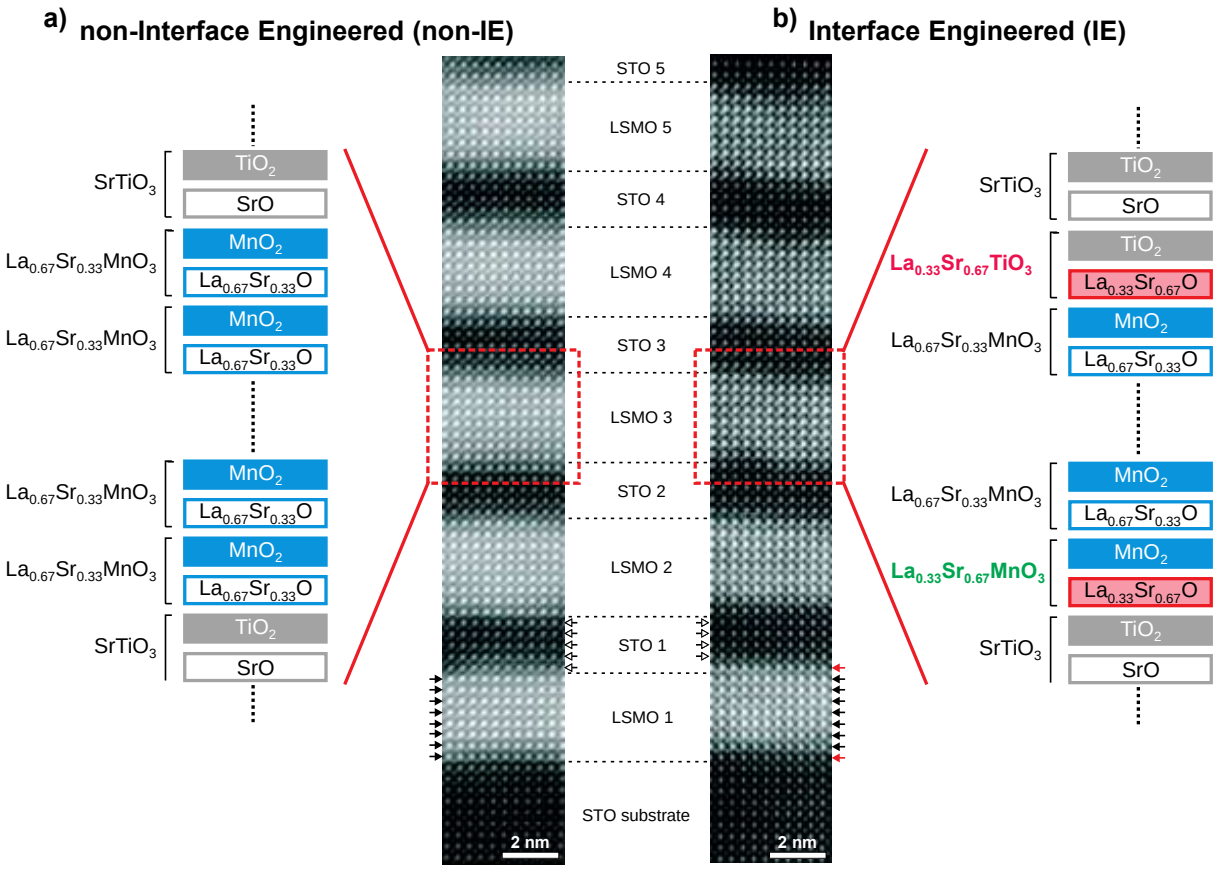

Figure 1. Scanning transmission electron microscopy analysis of LSMO/STO heterostructures (a) without and (b) with the insertion of $La_{0.33}Sr_{0.67}O$ layers for interface engineering. The $La_{0.67}Sr_{0.33}O$ layers (black arrows in LSMO), SrO layers (white arrows in STO) and $La_{0.33}Sr_{0.67}O$ layers (red arrows) are indicated.

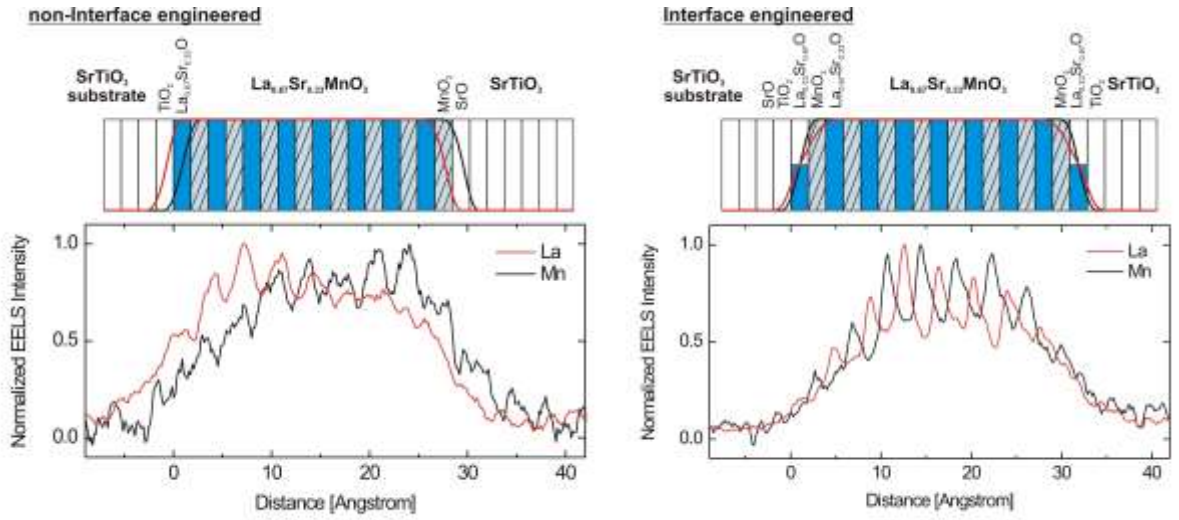

Figure 2. Electron energy loss spectroscopy (EELS) analysis of the LSMO/STO heterostructures for the (left) non-interface engineered and (left) interface engineered samples. Top: schematic representations of the atomic layering sequence for both types of heterostructures with La (red) and Mn (black) profiles. Bottom: Normalized core-loss signals for La $M_{4,5}$ (red) and Mn $L_{2,3}$ (black) edges.

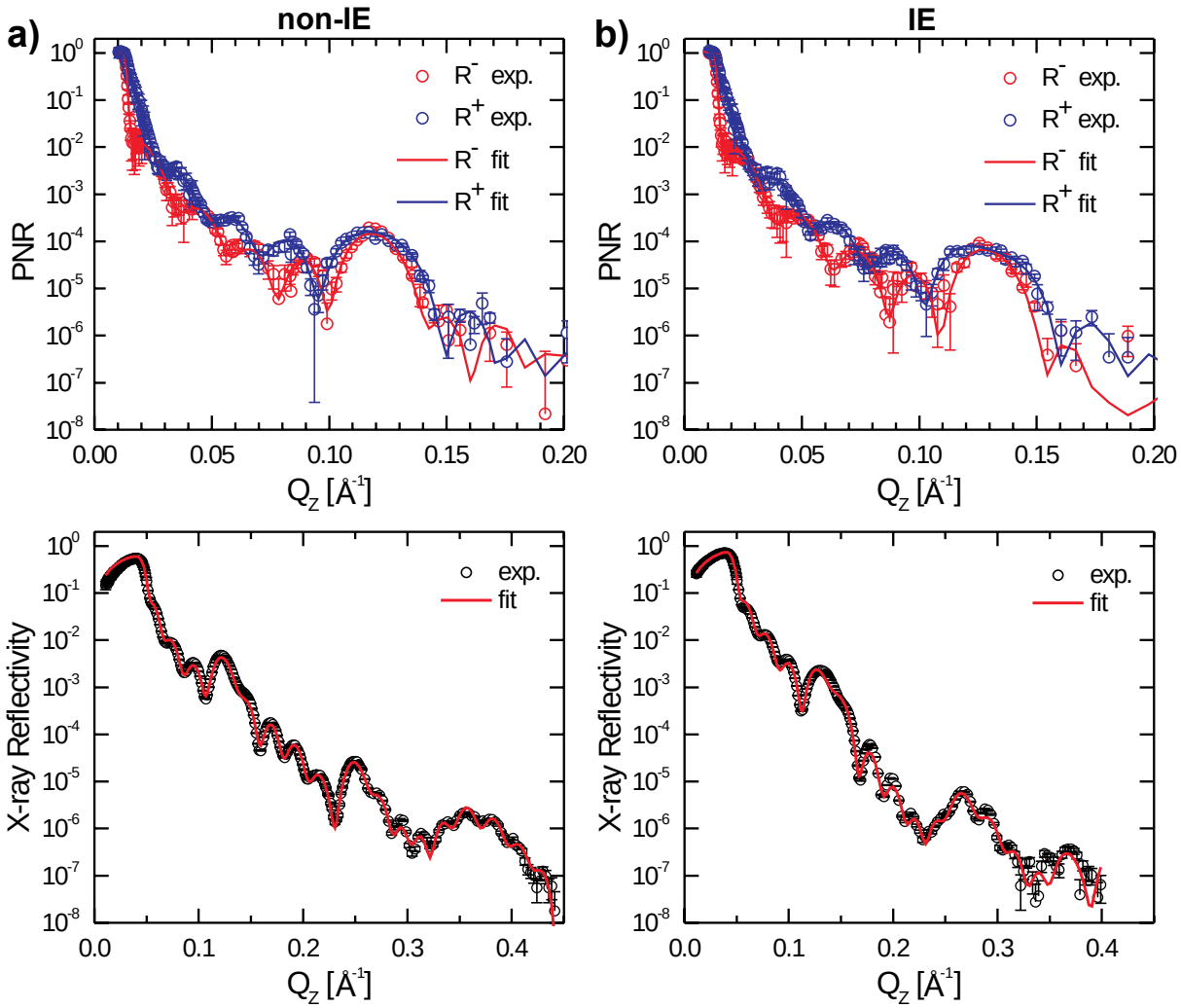

Figure 3. Neutron (top) and X-ray (bottom) reflectivity measurements of LSMO/STO heterostructures (a) without interface engineering (non-IE) and (b) with interface engineering (IE). Solid lines are the fits to the experimental data based on depth profile models of the scattering length densities. Neutron reflectivity for spin up (R^+) and spin down (R^-) polarized neutrons are shown.

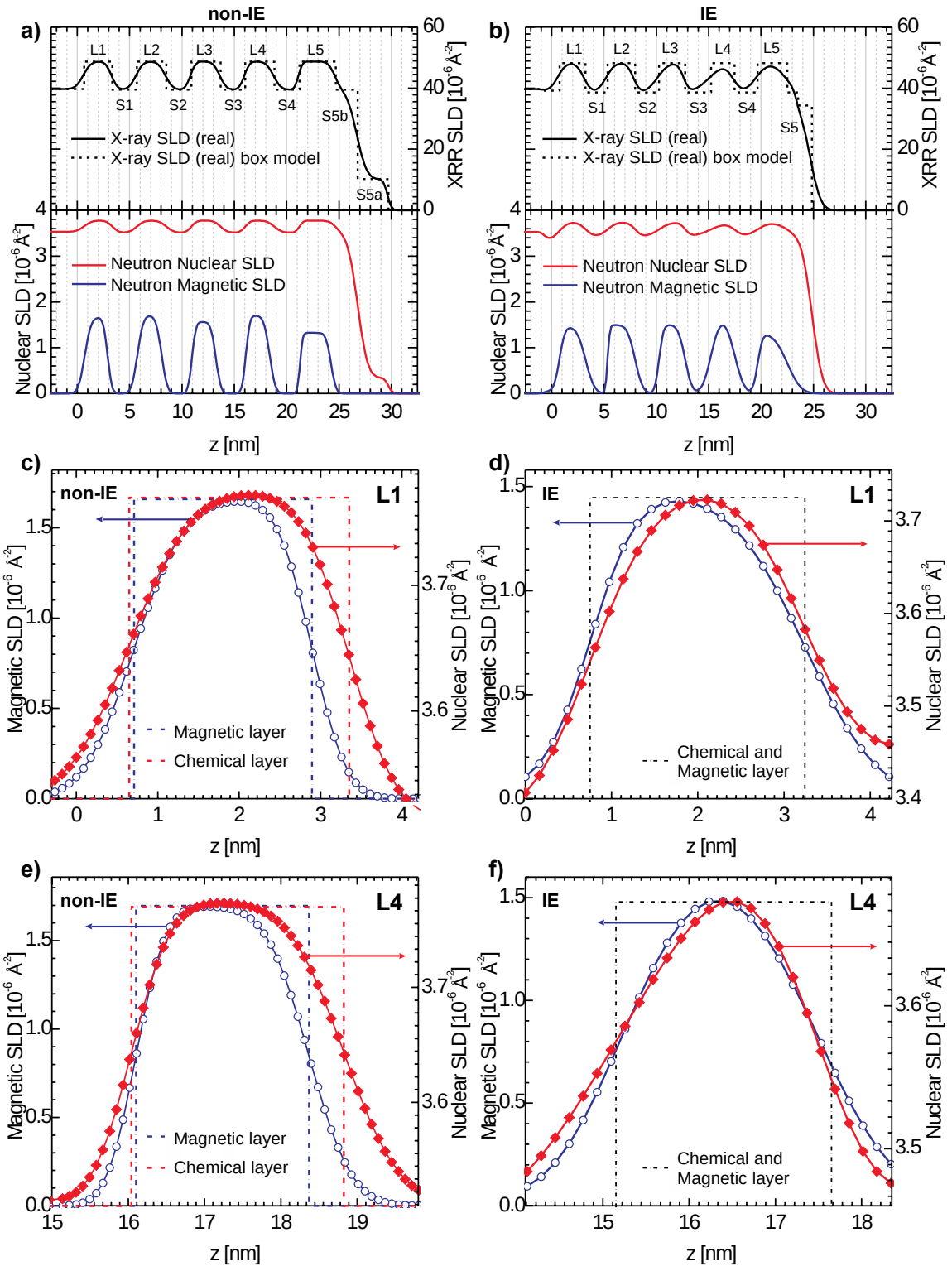

Figure 4. The magnetic and nuclear (chemical) scattering length density profiles at various film thickness *z* obtained from fitting the combined neutron and X-ray reflectivity data for LSMO/STO heterostructures (a) without and (b) with interface-engineering. The dashed lines represent the SLD profiles with sharp interfaces (a so-called box model). The individual LSMO (L1 to L5 from substrate to surface) and STO (S1 to S5) layers are indicated. (c,d,e,f) Overlay of the chemical and magnetic profile without (c,e) and with (d,f) interface-engineering for respectively the first (L1) and fourth (L4) LSMO layer.

Table of contents entry

Mark Huijben, Yaohua Liu, Hans Boschker, Valeria Lauter, Ricardo Egoavil, Jo Verbeeck, Suzanne G.E. te Velthuis, Guus Rijnders, and Gertjan Koster*

Enhanced local magnetization by interface engineering in perovskite-type correlated oxide heterostructures

Elimination of a magnetic dead-layer at the LSMO/STO interface has been achieved by interface engineering through incorporation of a single $La_{0.33}Sr_{0.67}O$ layer. Controlled growth of interfacial atomic stacking in combination with local magnetic probing by polarized neutron reflectometry has enabled controlled interface engineering and resulted in optimal interfacial magnetization in perovskite-type correlated oxide heterostructures.